JARO 16: 373–387 (2015)
DOI: 10.1007/s10162-015-0515-y

JARO
Journal of the Association for Research in Otolaryngology

Research Article

Histopathologic Changes of the Inner ear in Rhesus Monkeys After Intratympanic Gentamicin Injection and Vestibular Prosthesis Electrode Array Implantation

Daniel Q. Sun,[1,4] Mohamed Lehar,[1] Chenkai Dai,[1] Lani Swarthout,[1] Amanda M. Lauer,[1] John P. Carey,[1] Diana E. Mitchell,[3] Kathleen E. Cullen,[3] and Charles C. Della Santina[1,2]

[1]*Department of Otolaryngology-Head and Neck Surgery, Johns Hopkins University School of Medicine, Baltimore, MD, USA*

[2]*Department of Biomedical Engineering, Johns Hopkins University School of Medicine, Baltimore, MD, USA*

[3]*Department of Physiology, McGill University, Montreal, QC, Canada*

[4]*Department of Otolaryngology-Head and Neck Surgery, Johns Hopkins Outpatient Center, 6th floor, 601 North Caroline Street, Baltimore, MD 21287, USA*

Received: 17 November 2014; Accepted: 2 March 2015; Online publication: 20 March 2015

ABSTRACT

Bilateral vestibular deficiency (BVD) due to gentamicin ototoxicity can significantly impact quality of life and result in large socioeconomic burdens. Restoring sensation of head rotation using an implantable multichannel vestibular prosthesis (MVP) is a promising treatment approach that has been tested in animals and humans. However, uncertainty remains regarding the histopathologic effects of gentamicin ototoxicity alone or in combination with electrode implantation. Understanding these histological changes is important because selective MVP-driven stimulation of semicircular canals (SCCs) depends on persistence of primary afferent innervation in each SCC crista despite both the primary cause of BVD (e.g., ototoxic injury) and surgical trauma associated with MVP implantation. Retraction of primary afferents out of the cristae and back toward Scarpa's ganglion would render spatially selective stimulation difficult to achieve and could limit utility of an MVP that relies on electrodes implanted in the lumen of each ampulla. We investigated histopathologic changes of the inner ear associated with intratympanic gentamicin (ITG) injection and/or MVP electrode array implantation in 11 temporal bones from six rhesus macaque monkeys. Hematoxylin and eosin-stained 10-μm temporal bone sections were examined under light microscopy for four treatment groups: *normal* (three ears), *ITG-only* (two ears), *MVP-only* (two ears), and *ITG + MVP* (four ears). We estimated vestibular hair cell (HC) surface densities for each sensory neuroepithelium and compared findings across end organs and treatment groups. In ITG-only, MVP-only, and ITG + MVP ears, we observed decreased but persistent ampullary nerve fibers of SCC cristae despite ITG treatment and/or MVP electrode implantation. ITG-only and ITG + MVP ears exhibited neuroepithelial thinning and loss of type I HCs in the cristae but little effect on the maculae. MVP-only and ITG + MVP ears exhibited no signs of trauma to the cochlea or otolith end organs except in a single case of saccular injury due to over-insertion of the posterior SCC electrode. While implanted electrodes reached to within 50–760 μm of the target cristae and were usually ensheathed in a thin fibrotic capsule, dense fibrotic reaction and osteoneogenesis were each observed in only one of six electrode tracts examined. Consistent with physiologic studies that have demonstrated directionally appropriate vestibulo-ocular reflex responses to MVP electrical stimulation years after implantation in these animals, histologic findings in the present study indicate that although intralabyrinthine MVP implantation causes some inner

Correspondence to: Daniel Q. Sun · Department of Otolaryngology-Head and Neck Surgery · Johns Hopkins Outpatient Center, 6th floor · 601 North Caroline Street, Baltimore, MD 21287, USA. Telephone: 410-502-8048; email: dsun8@jhmi.edu

ear trauma, it can be accomplished without destroying the distal afferent fibers an MVP is designed to excite.

Keywords: vestibular prosthesis, vestibular implant, gentamicin, rhesus, macaque, intratympanic, transtympanic, cochlear implant

INTRODUCTION

The vestibular system helps maintain stable gaze and posture. Three semicircular canals (SCCs) in each ear encode head rotation while the saccule and utricle detect linear acceleration due to tilt or translation. Together, these end organs drive the angular vestibular-ocular reflex (VOR), vestibulo-ocular, vestibulospinal, and vestibulocervical pathways, among others (Carey and Della Santina 2010; Uchino et al. 1988; Wilson et al. 1990). Individuals who suffer profound unilateral vestibular hypofunction usually compensate well and regain nearly normal gaze and postural stability. However, individuals with severe or profound bilateral vestibular deficiency (BVD) typically experience chronic oscillopsia, disequilibrium, and postural instability. These disabling effects of BVD are associated with decreased quality of life and significant individual and socioeconomic cost (Sun et al. 2014). Causes of BVD include ototoxic drug exposure (most commonly due to aminoglycosides such as gentamicin), ischemia, infection, genetic abnormality, trauma, and others. There is currently no adequate therapy for patients who derive insufficient benefit from vestibular physical therapy and cessation of vestibular suppressants (Minor 1998; Brandt 1996).

Selective electrical stimulation of vestibular nerve branches to evoke directionally appropriate VOR eye movements is a promising therapeutic strategy for patients with BVD, and several single- (Gong and Merfeld 2000; Gong and Merfeld 2002) and multichannel vestibular prosthetic devices (Guyot et al. 2011; Rubinstein et al. 2012; Wall et al. 2007; Lewis et al. 2010; Della Santina et al. 2007a) have been developed. The multichannel vestibular prosthesis (MVP) developed in our laboratory encodes 3D head rotation and elicits VOR responses approximately aligned to ideal response directions when assayed using 3D oculographic techniques (Della Santina et al. 2007a; Fridman et al. 2010; Davidovics et al. 2013; Dai et al. 2013). These devices have successfully demonstrated surgical feasibility and functional restoration of VOR in rhesus monkeys. Recently, two groups have extended this approach to humans with BVD (van de Berg et al. 2012; Perez Fornos et al. 2014) or intractable Meniere's disease (Golub et al. 2014), with variable effects on VOR restoration and hearing.

Despite physiologic data (Rubinstein et al. 2012; Fridman et al. 2010; Davidovics et al. 2013; Perez Fornos et al. 2014; Stokroos et al. 2014; Rubinstein 2014; Dai et al. 2011a) demonstrating well-aligned electrically evoked vestibulo-ocular reflex (eVOR) responses, and intact hearing in rhesus monkeys treated with intratympanic gentamicin (ITG) to ablate the natural VOR and then implanted with MVP electrode arrays (Dai et al. 2011b), uncertainty remains regarding the status of the neuroepithelium after ITG injection and the extent of trauma caused by MVP electrode implantation. In contrast to the large body of evidence (Nadol and Eddington 2006; Nadol et al. 2008; O'Leary et al. 2013; Shepherd et al. 1984) on the biocompatibility and tolerability of cochlear implant electrodes and the incidence of unfavorable tissue responses to implantation trauma that could hinder implant performance, there is a paucity of published data on the occurrence and extent of adverse reactions to implantation of vestibular prosthesis electrodes. Only one published study (Lewis et al. 2010) has described histologic changes associated with vestibular prosthesis implantation for electrode arrays implanted in the temporal bones of two squirrel monkeys. In those two animals, ampullary nerves in all four implanted ears were described as qualitatively normal. However, those animals were normal prior to implantation and plugging of the horizontal SCCs, so data from that study could not reveal extent of injury due to multi-canal implantation with and without prior ototoxic injury.

In this study, we examined histopathologic changes in the inner ears of six rhesus monkeys after ITG injection alone at sufficient dose to ablate natural VOR responses to whole-body rotation, after ITG injection and subsequent MVP electrode implantation, and after MVP electrode implantation without prior ITG treatment. Specifically, we investigated the status of vestibular and cochlear neuroepithelia and their innervation, quantified anatomic relationships between implanted electrodes and neurons including both target and nontarget branches of the vestibulocochlear and facial nerves, and characterized the presence and extent of inflammation, infection, scar, and other tissue reactions to transmastoid implantation of MVP electrodes.

METHODS

Animals

Eleven temporal bones from six adult rhesus macaque monkeys (6–12 kg) were used in this study, which was

performed in accordance with a protocol approved by the Johns Hopkins Animal Care and Use Committee, accredited by the Association for the Assessment and Accreditation of Laboratory Animal Care International, and consistent with European Community Directive 86/609/EEC. These included three normal/untreated temporal bone specimens from three animals (*control*), two temporal bone specimens from two animals treated only with ITG (*ITG-only*), two temporal bone specimens from two animals treated with MVP electrode implantation without ITG (*MVP-only*), and four temporal bone specimens from three animals treated with both ITG and subsequent MVP electrode implantation (*ITG + MVP*). Each was harvested after euthanasia and transcardiac perfusion following completion of physiologic studies resulting in eVOR and hearing assessment data that have been published previously (Davidovics et al. 2013; Dai et al. 2013, 2011a, 2011b; Chiang et al. 2011; Mitchell et al. 2013). Diversity of physiologic study goals led to variation in the treatments to which each temporal bone was subjected. The nature and timing of interventions for each temporal bone studied is summarized in Table 1. In the two ITG-only temporal bones, time from final ITG treatment to euthanasia/perfusion varied between 20 days and 3 years. The two MVP-only temporal bones were from animals euthanized/perfused 18 to 19 months after implantation. The four ITG + MVP temporal bones underwent MVP implantation 5 days–4 months after final ITG treatment and were euthanized/perfused 3 years after implantation.

ITG Injection

Details of the ITG injection technique used in this study have been described previously (Dai et al. 2011a; Chiang et al. 2011). Briefly, ITG injection was performed transtympanically into the middle ear under general inhalational anesthesia (isoflurane 1–5 %). For each treatment, 0.3–0.5 mL of 26.7 mg/mL buffered gentamicin sulfate solution (67 % 40 mg/ml gentamicin sulfate, 20 % sodium bicarbonate, and 13 % sterile water) was instilled into the middle ear using a 25-gauge needle, and the animal remained under anesthesia with the treated ear up for 30 min after injection to promote diffusion of drug across the round window and into the inner ear. VOR responses were measured weekly after each treatment, and the treatment was repeated until VOR gain for responses during 1000 deg/s^2 whole-body transient rotations to a plateau of 150 deg/s in darkness toward the treated ear were <10 % of normal (Dai et al. 2013, 2011a). This required one injection in three ears, two in three ears, and five in one ear (due to apparent recovery of VOR requiring re-injection) (Table 1). Specimens in the ITG-only and ITG + MVP groups varied in the number and timing of ITG treatments, as is typical of subjects in series of human subjects treated with ITG for management of Meniere's disease (Nguyen et al. 2009; Chia et al. 2004). Histologic results of the ITG-only specimens therefore provide a useful and clinically relevant complement to the few human studies of the primate labyrinth's response to ITG.

MVP Implantation

MVP implantation was performed under general anesthesia (isoflurane, 3–5 %) via a transmastoid approach. Under sterile conditions, a mastoidectomy was performed and the junction of the horizontal and superior SCC (HSCC and SSCC) ampullae was identified. A fenestration in each bony canal was made near its ampulla, leaving a thin bone bridge as a landmark. A two-tined, forked electrode array containing three electrodes per tine to target the ampullary nerves of those SCCs was inserted (Chiang et al. 2011) (Appendix A). For the posterior SCC (PSCC), a fenestration was made in the thin segment of the bony canal near the ampulla and a second, single-tined electrode array containing three electrodes was inserted. A reference electrode was inserted in the common crus via a second PSCC fenestration. Throughout the procedure, care was taken to avoid violating the membranous labyrinth or suctioning perilymph. Pieces of fascia and bone were used to gently plug the fenestrations, and in some animals, dental cement was also used to stabilize the electrode arrays in the mastoid cavity, from which electrode leads were run in bone channels under periosteum to a connector within a dental acrylic head cap.

Euthanasia and Temporal Bone Preparation

Animals were euthanized under deep anesthesia via transcardial perfusion of physiologic saline and 2 % paraformaldehyde in four animals (F32RhD, M067RhF, F247RhE, and MRH37x) or 10 % formalin in two animals (M0603163RhO and M060323RhJ). Different fixative use resulted from institutional differences in euthanasia protocols. Temporal bones were then harvested and prepared in a process that is similar to that used for human specimens (Crowe et al. 1934). Briefly, each temporal bone was cut from the skull by a reticulating saw, post-fixed in 2 % paraformaldehyde, repeatedly trimmed while being decalcified in ethylenediaminetetraacetic acid (EDTA) and embedded in paraffin after dehydration through a series of ethanol baths. After decalcification and immediately prior to embedding in paraffin, MVP electrodes in implanted ears were carefully withdrawn

TABLE 1

Inner ear status of study animals

	Left ear		*Right ear*		
Animal	*Gentamicin*[a]	*MVP*	*Gentamicin*[a]	*MVP*	*Euthanasia/perfusion*
F32RhD	06/2009 10/2009	10/2009	04/2010	08/2012	11/2012
M067RhF	06/2010 06/2010	07/2010[b]	08/2010 09/2010 09/2013 09/2013 10/2013	None	10/2013
F247RhE	10/2009	11/2009 08/2011[c]	04/2010	None	03/2013
M0603163RhO	None	03/2012	Normal		09/2013
M060323RhJ	None	08/2010	Normal		03/2012
MRH37x	Normal		Not available		02/2013

MVP Multichannel vestibular prosthesis

[a]Intratympanic injection

[b]Posterior semicircular canal electrode pulled back after over-insertion

[c]Re-implantation after removal by animal

without additional surgical manipulation of the inner ear, since they would cause histologic trauma during sectioning. Embedded blocks were serially sectioned in a horizontal plane approximating the plane of the stapes superstructure at a slice thickness of 10 μm. Each slice was mounted on a glass slide and stained using hematoxylin and eosin (H&E).

Histopathologic Evaluation

H&E-stained sections were examined under light microscopy. Images at ×2.5 to ×40 magnification were acquired using a digital camera attached to the microscope with image acquisition software (ProgRes, Jenoptik). Figure 1 shows representative images of vestibular neuroepithelia under light microscopy with sufficient morphological detail to distinguish between types I and II hair cells (HCs). Consistent with commonly accepted morphologic criteria (Lysakowski and Goldberg 2008; Merchant 1999; Lyford-Pike et al. 2007), type I HCs were identified based on their flask shape and halo-like nerve calyx, whereas type II HCs were cylindrical and lacked a clear nerve chalice. To quantitatively evaluate the distribution of HCs in each vestibular end organ, we adopted methodologies developed by Merchant (Merchant 1999) for quantification of vestibular HCs in horizontally sectioned human temporal bones. For each vestibular end organ, a slice sampling fraction (ssf) was set a priori to minimize sampling bias, resulting in a median of five selected slices for each vestibular end organ. Selected slices were then captured at ×20 magnification and processed offline using Image J (NIH, Bethesda, MD). For each image, only the segment of neuroepithelium perpendicular to the plane of sectioning was used for analysis. Within this segment, all type I and II HCs were individually counted using a cell counter routine, and the ratio of the two cell types was calculated. Although the size of each image was constant (680×512 μm^2), the counting frame size was dependent on the length of intact neuroepithelium perpendicular to the plane of sectioning (range, 69–789 μm). Distinction was not made between central and peripheral zones for the SCC cristae or between striolar and non-striolar regions of otolith end organ maculae. For each image, the length and height (defined as the distance between the cuticular plate and the basement membrane) of the neuroepithelial segment as well as HC diameters were also measured. Neuroepithelial height was measured at the apex of each crista. The surface density of vestibular HCs was obtained by dividing the total cell count by the surface area, calculated as *length×thickness*, using a slice thickness of 10 μm and piecewise-linear approximations to the curved neuroepithelium surface. Consistent with Merchant (1999), the Abercrombie correction (1946) (Eq. 1) was used to correct for over-counting.

$$H_i = h_i \times \frac{t}{t+d} \quad (1)$$

where H_i=corrected HC density, h_i=counted HC density, t=section thickness, and d=nucleus diameter. Cell counts and measurements were tabulated and averaged across slices for each vestibular end organ of each ear. Results are presented as mean (standard deviation, SD). Student's t test (two-tail)

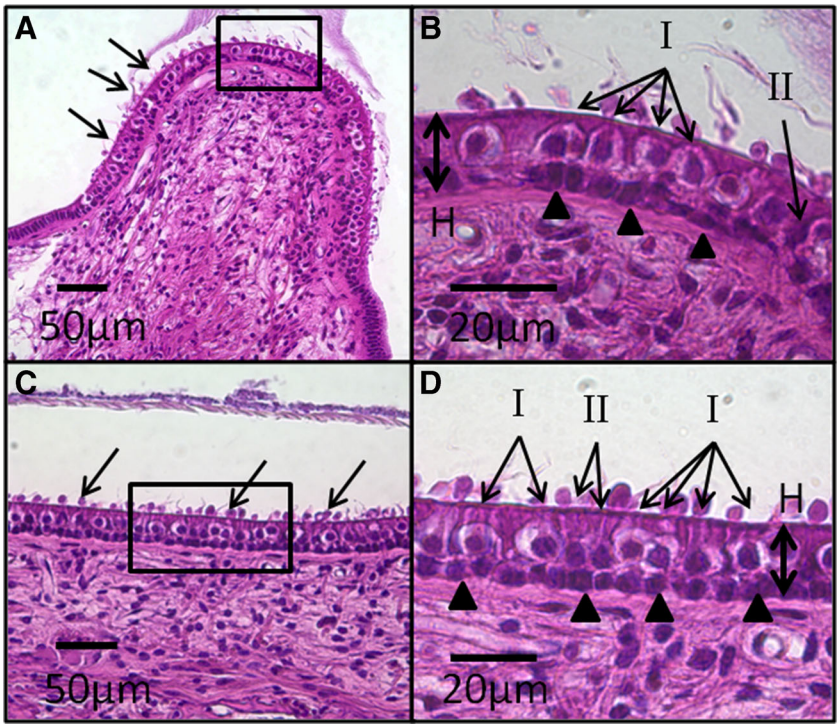

Fig. 1. Representative H&E-stained, light microscopy images of vestibular neuroepithelia from a normal control ear. SCC crista (**A**) neuroepithelium shows linear array of hair cells (*HCs*) and support cells arranged between the basement membrane and cuticular plate. Stereocilia (*arrows*) and cupula are visible. High magnification view (*box*) of the central zone of the crista (**B**) shows characteristic appearance of type I and II HCs. Type I HCs are flask shaped with spherical nuclei and surrounded by a single calyx that appears as a clear "halo," whereas type II HCs are cylindrical without a nerve chalice. Both type I and II HCs reside above a layer of supporting cell nuclei (*arrowheads*). The abundance of type I compared to type II HCs in the central zone of the crista is evident. The thickness of the neuroepithelium is measured from the basement membrane to the cuticular plate (*H*). A similarly cellular architecture is observed in the saccule macula (**C**). "Blebs" (*arrows*) occurring over the cuticular plate are a result of cellular autolysis during histologic processing. High magnification view (*box*) of the macula (**D**) again shows the distribution of type I and II HCs and support cells (*arrowheads*). The ratio of type I to II HCs is lower than that in the central zone of the crista shown in **B**.

was used to compare means between two groups, and one-way analysis of variance (ANOVA) with post hoc Tukey test was used to compare means between groups, with $P<0.05$ considered statistically significant (Stata 13, StataCorp).

RESULTS

Histopathology of SCC Cristae

Figure 2 shows representative images of SCC cristae for each treatment group. In *normal* ears (Fig. 2A–C), examination of H&E-stained sections under light microscopy showed normal neuroepithelia in the ampulla of each SCC. Type I and II HCs with associated stereocilia protruding from the cuticular plates and overlying a single row of supporting cell nuclei located along the basement membrane were distinctly visible. Although shrunken as a result of histologic processing, the cupula appears intact over each crista. In ITG-only ears (Fig. 2D–F), the apex of each SCC crista (correlating to the central zone) exhibited almost complete loss of HCs with only support cells remaining. There was associated loss of stereocilia and cuticular plate, resulting in a thin and mottled appearance for each neuroepithelium, as well as displacement or absence of the cupula. Associated with the almost total loss of sensory hair cells, ampullary nerve fibers to each crista were decreased in density in comparison to normal ears but still evident in each case. In MVP-only ears (Fig. 2G–I), SCC cristae showed variable histologic changes ranging from relatively normal with presence of HCs but diminished stereocilia (Fig. 2G), to near-total loss of stereocilia and HCs (Fig. 2H). In ITG + MVP ears (Fig. 2J–L), histologic changes resembled those observed in ITG-only ears, with significant loss of HCs, neuroepithelial thinning, absence or displacement of cupula, and decreased density but persistence of ampullary nerve fibers to each crista.

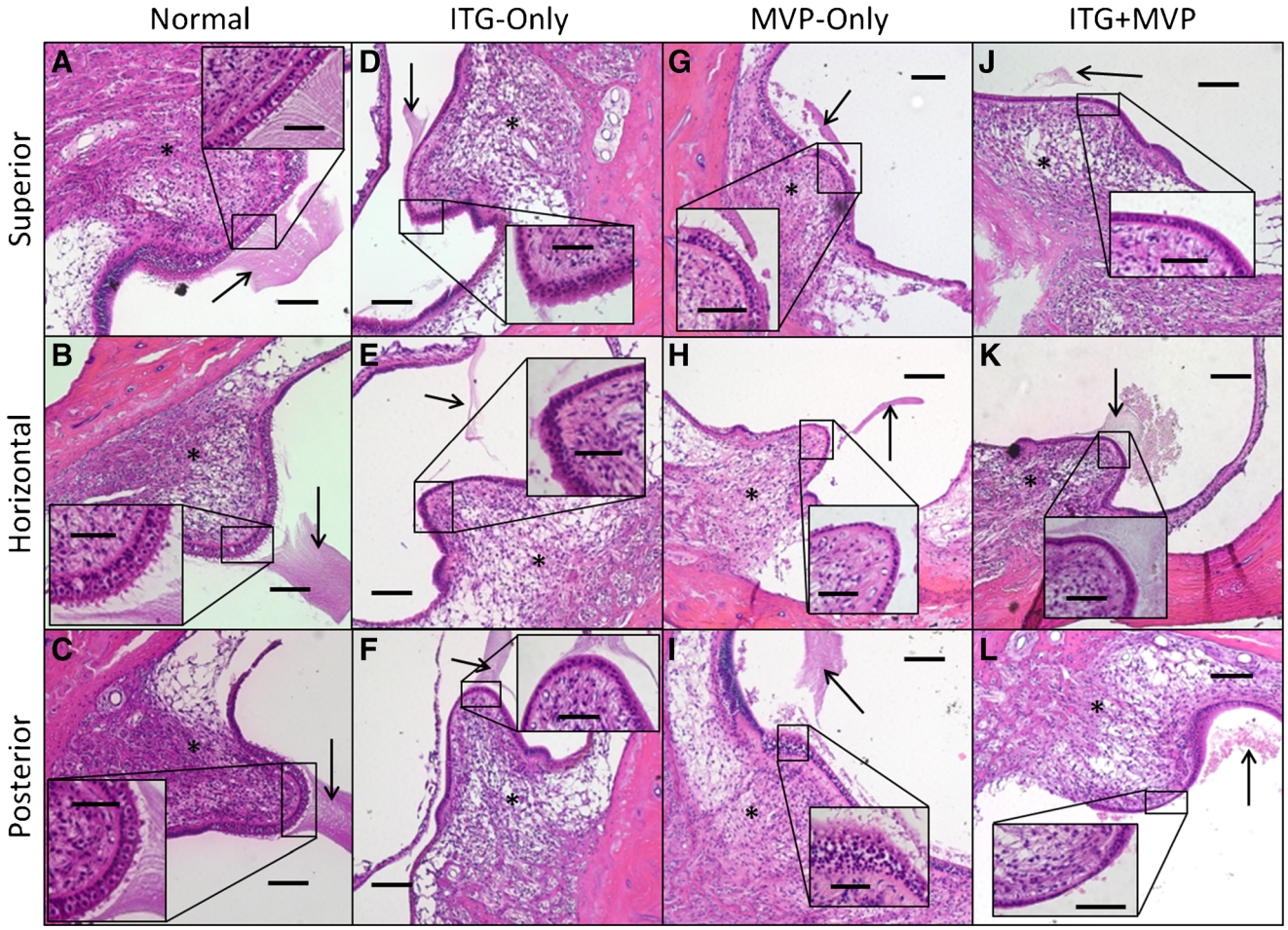

Fig. 2. Representative ×10 and ×40 (*inset*) light microscopy images of Rhesus monkey semicircular canal cristae. *Normal* ears (**A**–**C**) show a high ratio of type I to II hair cells (*HCs*) in the central zone of each crista, with intact stereocilia and cupula, and presence of ampullary nerve fibers. In *ITG-only* ears (**D**–**F**), there is almost complete loss of central zone HCs and stereocilia, with displacement of the cupula (*arrow*). The neuroepithelium is thinned and cuticular plate absent. There appears to be persistent innervation (*asterisk*) to each crista, albeit decreased in density, even up to 3 years (**D** and **E**) after final ITG injection and abolishment of angular vestibular-ocular reflex. In *MVP-only* ears (**G**–**I**), there is variable presence of type I and II HCs in the central zone. In *ITG + MVP* ears (**J**–**L**), there is consistent thinning of the central zone neuroepithelium with complete loss of type I and II HCs. Again, nerve fibers (asterisk) of each crista are evident. *MVP* multichannel vestibular prosthesis. *Scale bars* are 100 and 50 μm (*inset*). Specimens shown: MRH37x left ear for *normal*, F247RhE right ear for ITG-only, M0603163RhO left ear for MVP-only, and M067RhF left ear (**J**), F32RhD left ear (**K**), and F32RhD right ear (**L**) for ITG + MVP.

Histopathology of Otolith End Organ Maculae

Representative images of otolith maculae in study animals are shown in Figure 3. In normal ears (Fig. 3A, B), utricular and saccular maculae showed cellular architecture similar to normal SCC crista neuroepithelia, with type I and II HCs located above a single row of support cells. Stereocilia and otoconia were also visible. In ITG-only ears (Fig. 3C, D), type I and II HCs, associated stereocilia, and overlying otoconia continued to be present. In MVP-only ears (Fig. 3E, F), otolith maculae resembled those in normal and ITG-only ears, with intact neuroepithelium, stereocilia, and otoconia. In ITG + MVP ears, the maculae appeared similar histologically to other treatment groups except in a case of saccular trauma by an electrode array inserted ~3 mm beyond its intended target during PSCC ampullary implantation, which resulted in otoconial loss and macular thinning of that saccule (specimen M067RhF left ear, Fig. 3F). In this instance, the over-inserted PSCC electrode was pulled back in a subsequent operation. Neither fibrosis in the vestibule nor hydrops of the otolith organs was observed in any specimen.

Histopathology of Auditory Regions of the Temporal Bone

In MVP-only and ITG + MVP ears, gross examination revealed preservation of the ossicular chain, stapes

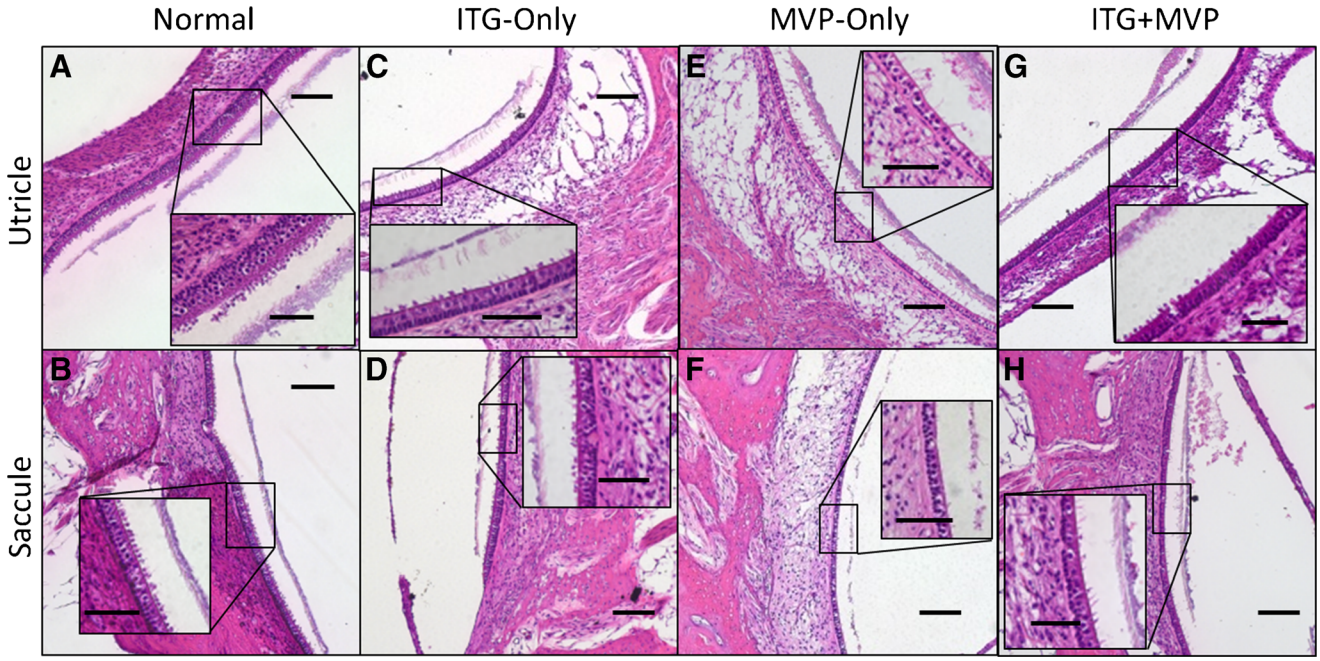

Fig. 3. Representative ×10 and ×40 (*inset*) light microscopy images of Rhesus monkey otolith end organ maculae. *Normal* ears (**A** and **B**) show utricular and saccular maculae with type I and II hair cells (*HCs*), intact stereocilia (*inset*), and presence of otoconia. In an *ITG-only* ear treated just 20 days prior to euthanasia, the utricular (**C**) and saccular (**D**) maculae both appear remarkably healthy, with minimal HC loss, preserved neuroepithelial height, and intact stereocilia and otoconia. This is in contrast to evidence of cristae injury from the same specimen in Figure 2D–F. In *MVP-only* ears (**E** and **F**), or those that received ITG injection followed by MVP implantation (**G** and **H**), preservation of HCs, stereocilia, and otoconia are again demonstrated. However, in an ear with surgical trauma to the saccule as a result of PSCC electrode insertion (**F**), thinning of the neuroepithelium and overlying otoconia, with decreased HCs and almost complete loss of stereocilia, is observed. *MVP* multichannel vestibular implant. *Scale bars* are 100 and 50 μm (*inset*). Specimens shown: MRH37x left ear for *normal*, M067RhF right ear for ITG-only, M0603163RhO left ear for MVP-only, and M067RhF left ear (**G**) and F32RhD right ear (**H**) for *ITG + MVP*.

footplate, and cochlea. Histologic examination also revealed preservation of cochlear structures such as inner and outer HCs, tectorial membrane, and scalae tympani and vestibuli (Fig. 4). These findings were also consistent with those observed in normal and ITG-only ears.

Quantitative Analysis of SCC Cristae and Otolith end Organ Maculae

Quantitative analysis of each vestibular neuroepithelium corroborated the qualitative histopathologic observations described above. Figure 5

Fig. 4. Representative image of stapes footplate and cochlea in a rhesus monkey that underwent intratympanic gentamicin (*ITG*) injection and MVP implantation. Image of the oval window (**A**) shows intact stapes footplate (*arrow*, folding due to histologic artifact) and adjacent structures, including facial nerve (*FN*), cochlea (*Co*), incus (I, fractured during histologic processing), utricle (*U*), and saccule (*S*). Cochlea (**B**) in the same animal also appears grossly intact. Inset (**C**) shows scala tympani (*ST*), scala vestibuli (*SV*), and scale media (*SM*). Intact tectorial membrane (*arrowhead*), inner, and outer hair cells (*arrows*) are visible. Light microscopic images of H&E-stained tissue acquired under ×2.5–×20 magnification. *Scale bars* are 500 μm (**A** and **B**) and 100 μ (**C**). Specimen shown: F32RhD right ear.

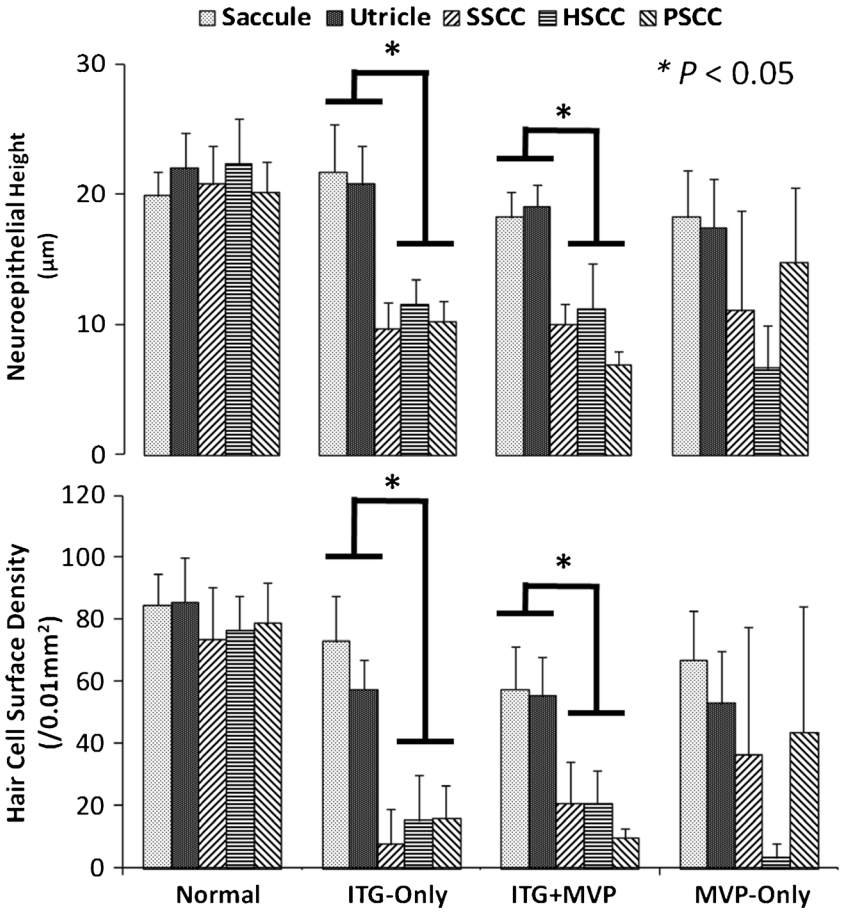

Fig. 5. Neuroepithelial height (*top*) and vestibular hair cell (*HC*) surface density (*bottom*) of each vestibular end organ for each treatment group. Compared to *normals, ITG-only* ears showed a decrease in neuroepithelial height and HC density in the semicircular canal (*SCC*) cristae, but not in the otolithic end organ maculae. Similarly, in *ITG + MVP* ears, the ototoxic effects of gentamicin appeared to be attenuated in otolith maculae compared to SCC cristae. Variability in HC density and neuroepithelial height in *MVP-only* ears reflects spectrum of surgical trauma.

shows the height and vestibular HC surface density of each neuroepithelium for each treatment paradigm. Normal ears had mean total HC surface densities of 84.6±10.0 (mean±standard deviation), 85.5±14.7, 73.7±16.6, 76.6±11.0, and 78.6±13.2 HCs/0.01 mm^2 in the saccule, utricle, SSCC, HSCC, and PSCC, respectively. Across all normal cristae and maculae, the mean type I to II HC density ratios were 2.3±0.8 and 1.1±0.4, respectively (T_{81}=9.42, P<0.001). In ITG-only ears, compared to SCC cristae, the otolith maculae contained significantly greater HC surface density (one-way ANOVA, $F_{5,44}$=52.20, P<0.001; Tukey's multiple comparison test: P<0.01 between each crista and macula) and larger neuroepithelial height (one-way ANOVA, $F_{5,44}$=47.20, P<0.001; Tukey's multiple comparison test: P<0.01 between each crista and macula). Mean type I to II HC ratios were 1.5±0.8 and 1.4±0.3 in ITG-only cristae and maculae, respectively (T_{21}=0.31, P=0.76). Comparing ITG-only to normal cristae, the decreased type I to II ratio in ITG-only cristae (T_{32}=4.04, P<0.001) suggests selective loss of type I HCs. In MVP-only ears, there was variable preservation of neuroepithelial height and HC surface density between vestibular end organs due to varying degrees of electrode trauma. In ITG + MVP ears, HC density (one-way ANOVA, $F_{5,39}$=28.73, P<0.001; Tukey's multiple comparison test: P<0.01 between each crista and macula) and neuroepithelial height (one-way ANOVA, $F_{5,39}$=64.78, P<0.001; Tukey's multiple comparison test: P<0.01 between each crista and macula) were attenuated in the SCC cristae relative to otolith end organ maculae, similar to observations in ITG-only ears.

Histopathology of Electrode Tracts

Because electrode arrays were necessarily withdrawn from each specimen prior to sectioning, we assayed histopathologic changes associated with electrode insertion in temporal bones that received MVP implantation by examining the fibrous capsules left behind after electrode removal. Within each SCC, electrode tracts were typically characterized by thin fibrous capsules that were within 760 μm of the target crista as measured on

histologic sections (e.g., Fig. 6A, B). One implanted ear exhibited evidence of osteoneogenesis around an electrode tract (M0603163RhO left ear, Fig. 6C) while another had a vigorous fibroblastic response around the electrode tract in the PSCC ampulla (F32RhD left ear, Fig. 6D). We did not observe extension of scar tissue beyond the ampulla into the vestibule, on the stapes footplate, or in the cochlea in any ear. However, all implanted specimens showed signs of either pre- or post-mortem tissue damage, which typically consisted of shearing and/or destruction of the crista. In some cases, cell-level findings clearly indicate pre-mortem damage. For example, Figure 6B shows the complete loss of both HSCC and SSCC crista. In other cases, relative preservation of cellular architecture despite the presence of a cleavage plane across a structure suggests post-mortem damage due to electrode removal during histologic processing. Figure 6D shows partial shearing of the PSCC crista, apparently as a result of electrode removal. In both MVP-only and ITG + MVP ears, ampullary nerves were present at the site of stimulation despite injury to the overlying crista. Neither bacteria, polymorphonuclear inflammation, nor granulomatous giant cell reactions were observed in any specimen.

DISCUSSION

Effects of Intratympanic Gentamicin on the Labyrinth

Histopathologic changes observed in this study provide an anatomic context for interpretation of physiologic data previously reported for the same animals (Davidovics et al. 2013; Dai et al. 2013, 2011a, 2011b; Mitchell et al. 2013). Consistent with previous studies in rodents (Lyford-Pike et al. 2007; Hirvonen et al. 2005; Lopez et al. 1997), we observed loss of type I HCs in the central zone of each rhesus SCC crista after ITG injection, indicated by a decrease in type I:II HC ratio from 2.3 in normal ears to 1.5 in ITG-only ears. The ototoxic effects of ITG appear to be less severe in the otolith maculae, however, as we observed relative preservation of neuroepithelial height, HC density, and type I:II HC ratio in ITG-treated maculae compared to normal ears. Although not previously

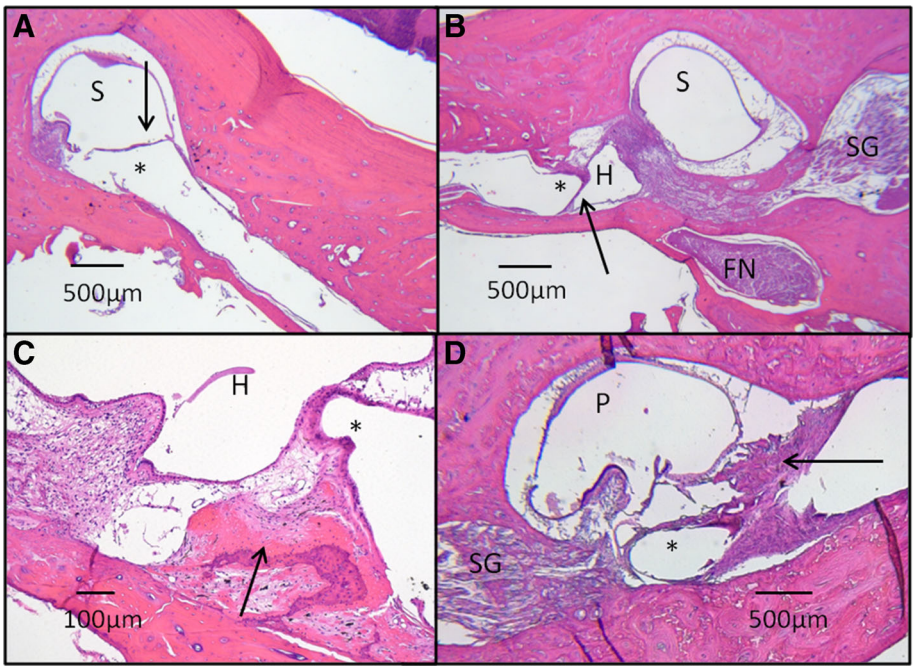

Fig. 6. Histopathology of electrode array tracts. Typically, a thin fibrotic capsule (*arrow*) surrounds the electrode tract (*asterisk*), terminating adjacent to an superior semicircular canal (*SSCC*) crista (**A**). The electrode tract is seen traversing through the surgical fenestration into the SSCC ampulla (*S*). In **B**, the orientation of an horizontal semicircular (*HSCC*) electrode tract (*asterisk*) and its fibrous capsule (*arrow*) are seen in relation to other adjacent structures, including the HSCC ampulla (*H*), SSCC ampulla (*S*), facial nerve (*FN*), and Scarpa's ganglion (*SG*). The close proximity of the HSCC electrode tract to the SSCC ampullary nerve is evident, demonstrating the anatomic basis for current spread between HSCC and SSCC ampullary nerves. In one monkey (**C**), osteoneogenesis (*arrow*) was found adjacent to an electrode tract (*asterisk*) in the HSCC ampulla (*H*). In another monkey (**D**), a vigorous fibrosis reaction (*arrow*) is seen adjacent to a posterior semicircular canal (*P*) electrode tract (*asterisk*). Osteoneogenesis and fibrosis may be due to electrode insertion or surgical placement of bone paté and/or fascia around labyrinthotomies during implantation. In all specimens, existent ampullary nerve innervation to crista was evident, even in cases that suffered surgical destruction of the crista during implantation (**B**). There was no evidence of granulomatous inflammation, hydrops, or extension of fibrosis into the vestibule in any specimens. H&E-stained images captured at ×2.5–×10 magnification under light microscopy. Specimens shown: M0603163RhO left ear (**A** and **C**), F32RhD right (**B**), and left (**D**) ears.

demonstrated in rhesus monkeys, attenuation of aminoglycoside ototoxicity in the otolith organs has also been observed in other mammals. Similar findings have been reported with streptomycin in cat (Wersall and Hawkins 1962), squirrel monkey (Igarashi et al. 1965), and guinea pig (Lindeman 1969) and with gentamicin in guinea pig (Sera et al. 1987) and rabbit (Kim et al. 2013). In humans, one study observed less decrease in HC density in the utricular macula compared to SCC crista after ITG injection for Ménière's disease in one patient (Ishiyama et al. 2007). Other human temporal bone histopathology studies have also found relative sparing of otolithic maculae in cases of systemic aminoglycoside ototoxicity (Nadol 1981; Schuknecht 1993; Tsuji et al. 2000). Proposed mechanisms of otolithic sparing include decreased HC sensitivity in the macula and/or regeneration or repair following injury (Baird et al. 1993; Golub et al. 2012; Carey et al. 1996). It is worth noting that in the one animal of the present study that was euthanized only 20 days after final ITG treatment, both the utricular and saccular maculae appeared healthy and intact (Fig. 3A, B) despite abolishment of physiologic VOR. In this instance, the time elapsed between ITG treatment and sacrifice was short enough that the relatively normal appearance of the maculae compared to the cristae is unlikely to be due to ototoxic injury (which typically manifests in symptoms and signs of acute vestibular loss about 1–2 weeks after ITG in rhesus and human (Carey 2004)) followed by regeneration or repair. Since prospective, quantitative physiologic measurements of postural reflexes or VOR to head translation were not performed to interrogate otolith function in these animals (which were implanted with electrodes intended to stimulate the SCCs, not the otolith end organs), the physiologic significance of these histopathologic findings awaits further investigation. Moreover, since tissues were not prepared for electron microscopy, whether differential calyceal changes exist in the crista compared to the macula as reported in rodents (Lopez et al. 1997) could not be determined.

Effects of MVP Electrode Implantation on the Labyrinth

Histologic exams in this study revealed electrode tracts within 50–760 μm of the targeted crista in each SCC of each animal, providing histologic corroboration of previously reported VOR data in these animals (Davidovics et al. 2013; Dai et al. 2013, 2011a; Chiang et al. 2011). Apart from the proximity of an electrode to its target nerve branch, the relative distance from an electrode to target vs nontarget ampullary nerves is a key determinant of 3D eVOR performance because restoration of a directionally appropriate 3D VOR requires selective stimulation of the target ampullary nerve and minimization of current spread to nontarget neurons. The anatomic proximity of HSCC and SSCC ampullary nerves is such that achieving selective stimulation of one without inadvertently exciting the other has been a central challenge in designing electrode arrays, implantation techniques and stimulation protocols (Fridman et al. 2010; Della Santina et al. 2005; Della Santina et al. 2007b; Davidovics et al. 2011). In one specimen (F32RhD/right), the HSCC electrode capsule was situated 452 and 928 μm from the targeted HSCC and SSCC ampullary nerves, respectively, representing a difference in distance of only 476 μm (Fig. 6B).

Although prior studies have not found evidence of neuronal loss in Scarpa's ganglion in human temporal bones after aminoglycoside ototoxicity (Tsuji et al. 2000), uncertainty exists regarding whether ampullary nerves may serve as viable targets of stimulation in subjects who have suffered ototoxic injury, consequent HC loss, and possible ampullary nerve degeneration (van de Berg et al. 2012; Wall et al. 2002). In this series of rhesus monkeys, those that received ITG injection (ITG-only) with near complete ablation of physiologic VOR (Davidovics et al. 2013; Dai et al. 2013, 2011a; Chiang et al. 2011) demonstrated histologic evidence of decreased but persistent ampullary nerve fibers associated with each crista despite loss of HCs in the overlying neuroepithelium (Fig. 2D–F, J–L). In fact, presence of ampullary nerve fibers was evident even 3 years after ITG treatment sufficient to cause profound loss of VOR (Fig. 2D, E).

Two different surgical approaches to position stimulating electrodes near their target ampullary nerves have been reported: intralabyrinthine and extralabyrinthine. The former has effectively become the de facto standard used by all three currently active research groups performing vestibular electrode implantation (van de Berg et al. 2012; Perez Fornos et al. 2014; Golub et al. 2014; Dai et al. 2011a). The latter, which Kos et al. (2006) proposed and called the "extraampullar" approach, involves attempts to access each ampullary nerve branch, without opening the labyrinth, by performing a lateral approach to the PSCC ampullary nerve just below the round window (previously described by Gacek and Gacek (2002) to accomplish singular neurectomy for control of intractable PSCC benign paroxysmal positional vertigo) and a separate superolateral approach to the superior and horizontal SCC's ampullary nerves. That approach has largely been abandoned due to the risks it poses to the tympanic segment of the facial nerve in humans (Stokroos et al. 2014); however, it would merit reconsideration if histologic exams of ears implanted by the intralabyrinthine approach were to reveal neuronal degeneration to such an extent that target neurons no longer extend their distal axons into the cristae near which intralabyrinthine electrodes are placed (Wall et al. 2002). The intralabyrinthine approach can be further specified as either *ampullary*—in which electrode arrays are deliberately inserted into each ampulla, with an intent to place them close to target neurons at the expense of

membranous labyrinth disruption (as was done here)—or *thin segment*, in which the surgeon creates a small opening in each SCC's thin segment and then advances electrode arrays toward each crista while attempting to avoid disruption of the membranous labyrinth. Histologic evidence of persistent ampullary innervation and lack of trauma to the auditory regions of the temporal bone in MVP-only and ITG + MVP ears in the present study support the use of the ampullary surgical approach employed here and apparently render the extralabyrinthine approach unnecessary when the goal is to position electrodes near their targets while avoiding loss of vestibular afferents and cochlear trauma.

The surgical technique and electrodes employed in this study appear not to engender a significant inflammatory response. The lack of inflammatory tissue reactions to MVP electrode implantation in this series is consistent with histologic findings in two implanted ears from two squirrel monkeys implanted with similar electrode arrays (Lewis et al. 2010) and observations from the human cochlear implant (CI) experience. Based on animal and human post-mortem studies, CI electrode implantation in the scala tympani typically elicits fibrosis with capsule formation (Nadol and Eddington 2006; O'Leary et al. 2013; Shepherd et al. 1984). Osteoneogenesis and dense fibrosis around the electrode capsule, which were each observed in one ear in the current study, may have occurred as a result of tissue reaction to electrode insertion or the surgical placement of autologous graft materials consisting of bone paté and/or fascia around labyrinthotomies for stabilization of electrode arrays, during implantation. In the present study, the two ears with osteoneogenesis and dense fibrosis had MVP implants in place for 1 and 3 years, respectively. In contrast, human studies described these effects 10–12 years after cochlear implantation (Nadol and Eddington 2006; Shepherd et al. 1984), although the post-mortem nature of these studies precludes accurate determination of time-to-occurrence. Other histopathologic changes associated with CI insertion include granulomatous and foreign body giant cell reaction (Nadol et al. 2008; O'Leary et al. 2013), cellular inflammation associated with bacterial inoculation (Shepherd et al. 1984), and hydrops (Tien and Linthicum 2002). Such changes have been theorized to play a role in "soft" failures after cochlear implantation (Nadol et al. 2008) or to cause other deleterious effects on inner ear function (Tien and Linthicum 2002), but no such changes were observed in the present study. This may be partially attributable to the small sample size, use of sterile technique, and the fact that the aforementioned histopathologic changes seen in some CI cases occur on time scales that could not be captured in the present study. For instance, foreign body giant cell reactions are more likely to occur early after implantation (4 weeks after cochlear implantation in guinea pigs) (O'Leary et al. 2013), whereas osteoneogenesis may appear years later (Nadol and Eddington 2006).

Trauma observed in implanted specimens may be an effect of surgery (e.g., disruption of structures as a direct result of electrode array insertion) or histologic artifact (e.g., due to post-mortem removal of electrodes for tissue processing). Apparent stability of VOR responses during life and the post-mortem presence of afferent axons suggest that much of the observed tissue damage may be attributable to post-mortem processing rather than surgery or electrode insertion. The temporal bone sectioning technique employed in this study required the withdrawal of electrode arrays immediately prior to sectioning, which may lead to disruption of anatomical structure in proximity to the electrode tracts. Shearing and/or destruction of the crista observed in certain specimens on histology are consistent with the degree of surgical or histologic processing trauma observed in a previous study utilizing squirrel monkeys (Lewis et al. 2010).

Effects of MVP Electrode Implantation on the Cochlea

A previous study on hearing outcomes after unilateral left ear ITG and MVP implantation employing animals F32RhD, M067RhF, and F247RhE showed a maximum 10 dB decrease in hearing thresholds as measured by auditory brainstem reflex (ABR) to clicks and 1–4 kHz tone bursts and 2–14 dB decrease on distortion product otoacoustic emissions (DPOAE) for 1–4 kHz stimuli in the implanted ear (Dai et al. 2011b). The histopathologic changes observed in this study corroborate those findings. There was no evidence of surgical disruption or scar tissue formation in auditory regions of the inner ear, such as the cochlea and oval window, in those specimens, and osteoneogenesis was either absent or confined to the area where bone dust was used to facilitate closure of the surgical entry into a canal.

Effects of Hair Cell Counting Technique

In estimating vestibular HC densities in study ears, the Abercrombie correction (Abercrombie 1946) was used to correct for over-counting. While less rigorous than the dissector stereological technique (Sterio 1984), its accuracy has been validated in multiple studies of archived human temporal bones that underwent sectioning and processing using techniques similar to those employed in this study (Merchant 1999; Richter 1980; Rauch et al. 2001), and yielded results similar to more labor-intensive stereological methods (Lopez et al. 2005). Moreover, although optical (Severinsen et al. 2010) and physical dissector techniques (Lysakowski and Goldberg 2008) have been employed with success

in other studies, pilot studies in our specimens indicated that the slice thickness we employed (10 μm) was too thin for optical sectioning and too thick for physical dissector techniques, relative to the average size of an HC (5 μm). The typical nucleus size was measured in each section and found to be comparable across all tissues examined, minimizing the effect of varying nucleus size on cell estimates. Moreover, since unbiased stereology relies on unbiased sampling of the anatomic area of interest in a uniform plane of section, its application to labyrinthine tissues such as those in this study would have had limited value when competing histologic goals require that one serially section the entire labyrinth in a single, fixed orientation. For instance, due to the fixed plane of sectioning, only a small fraction of a certain region is available for counting (e.g., 8 % of utricle when sectioned in the axial plane) (Merchant 1999). In fact, where unbiased stereological methods have been successfully applied to vestibular neuroepithelia, each neuroepithelium of interest was microdissected before sectioning to ensure that the sectioning plane was perpendicular throughout the region of interest to maximize yield (Ishiyama et al. 2007; Lopez et al. 2005; Gopen et al. 2003). This was not possible in the present study, as it would have led to the destruction of anatomical areas of interest relevant to MVP implantation.

Total HC surface density in the cristae and maculae has been shown to decrease with increasing body size, being approximately 120–200/0.01 mm^2 in chinchillas (Fernandez et al. 1995; Desai et al. 2005a; Desai et al. 2005b), 100–130/0.01 mm^2 in squirrel monkeys (Fernandez et al. 1995), and 60–80/0.01 mm^2 in humans (Richter 1980; Lopez et al. 2005). Although normative data have not been published for the rhesus monkey, the mean total HC estimate of 79/0.01 mm^2 (SD 3.0/0.01 mm^2) we measured for cristae and maculae of normal rhesus ears in this study is consistent with this trend when compared to human and small animal data obtained using unbiased stereology.

The mean type I:II HC ratios of 2.3 (SD 0.8) and 1.1 (SD 0.4) in the crista and macula, respectively, estimated in this study are in range of ratios of approximately 1.6–2.4 in the central zone of the crista (Rauch et al. 2001; Lopez et al. 2005) and 1.4–1.7 in the otolith end organ macula (Gopen et al. 2003; Merchant et al. 2000) in humans. Methods employed in this study cannot consistently distinguish between the central and peripheral zones in the cristae or striolar and nonstriolar regions in the maculae. In normal humans, there is decreased HC density in the central zone and striolar region (Lopez et al. 2005; Gopen et al. 2003) and increased type I:II HC ratio in the central zone (Lopez et al. 2005). Although consistent with our qualitative observations, these differences could not be quantified in the present study due to the lack of well-defined anatomic boundaries. Therefore, estimates reported here represent gross estimates of the entire neuroepithelium.

Study Limitations

The whole-temporal bone sectioning approach and tissue staining techniques employed for histologic study prevented rigorous quantification of ampullary nerve fibers in ears with and without MVP implantation via axonal counts and verification via immunohistochemistry. Loss of afferents may also be underestimated due to the limited time span between ITG injection and sacrifice in some animals. Indeed, in ears that were exposed to ototoxic treatment or surgical trauma, it is not surprising that loss of overlying neuroepithelium may lead to consequential loss of afferent nerve fibers. The number of residual nerve fibers, specific extent of retraction of their nerve terminals, or the Scarpa's ganglion cell bodies from which these fibers originate, could not be quantified in the present study. Moreover, in instances where persistence of ampullary fibers was observed, changes to their terminal structures as a result of loss or injury of the overlying HCs may have important implications for prosthetic stimulation and await further investigation.

This study is also limited by its retrospective nature and sample size. Since animals were studied in the context of an iterative process of MVP device development, interventions were heterogeneous and uncontrolled with respect to histopathologic evaluation. Furthermore, because the use of paraffin as an embedding medium prevented sectioning of temporal bones with electrodes in situ without sustaining a large degree of histologic trauma on native tissues, position of electrodes was necessarily inferred from examination of the fibrotic capsule surrounding electrode tracts, which may not reflect the true position of electrode arrays during physiologic experiments. Finally, the observed osteoneogenesis and fibrosis may not reflect tissue reaction to electrode insertion but rather placement of free grafts for electrode stabilization. Unfortunately, the extent to which bone chips, bone pate, and/or fascia were used was variable and was not documented in the surgical record with sufficient precision to permit a rigorous comparison between cases with and without deliberate insertion of such grafts. Despite these caveats,

our findings nonetheless provide histopathologic correlates to MVP electrode implantation in the temporal bone.

CONCLUSION

In a series of six rhesus monkeys that underwent ITG injection and/or MVP implantation, histologic exams demonstrated that ITG injection at doses sufficient to result in near-total ablation of VOR responses to high-acceleration ipsiversive whole-body rotation was associated with HC loss in the SCC cristae but less impact on the otolith end organ maculae, raising important clinical implications regarding the use of ITG for treatment of Ménière's disease and the role of ITG in creating animal models for the study of unilateral vestibular loss. Observations also demonstrated the safety of MVP implantation via a transmastoid, intralabyrinthine, ampullary approach, with minimal histopathologic impact on inner ear structures occurring beyond each implanted SCC crista ampullaris. Moreover, histologic examination revealed decreased but persistent ampullary nerve fibers near the stimulating electrodes despite prior ITG treatment, electrode implantation, and delivery of prosthetic currents in repeated sessions for up to 3 years, further strengthening the scientific foundation for efforts toward developing MVP devices intended to stimulate vestibular afferents in humans disabled by BVD.

ACKNOWLEDGMENTS

Custom electrode arrays for this study were produced by Roland Hessler (MedEl GmbH) and Frank Risi (Cochlear Corp.), to whom the authors express their gratitude. This work was funded by the National Institute on Deafness and Other Communication Disorders (NIDCD) R01DC009255, R01DC002390, and P30DC005211 and by contributors to the Johns Hopkins Vestibular NeuroEngineering Lab Research Fund.

Conflict of Interest

CCDS holds an equity interest in and is an officer of Labyrinth Devices, LLC. He has been a consultant to Cochlear Corporation and is currently a consultant to MedEl GmbH and Novartis Institutes for BioMedical Research, Inc. The terms of these arrangements are managed by The Johns Hopkins University Office of Policy Coordination in accordance with university policies on potential conflicts of interest.

APPENDIX

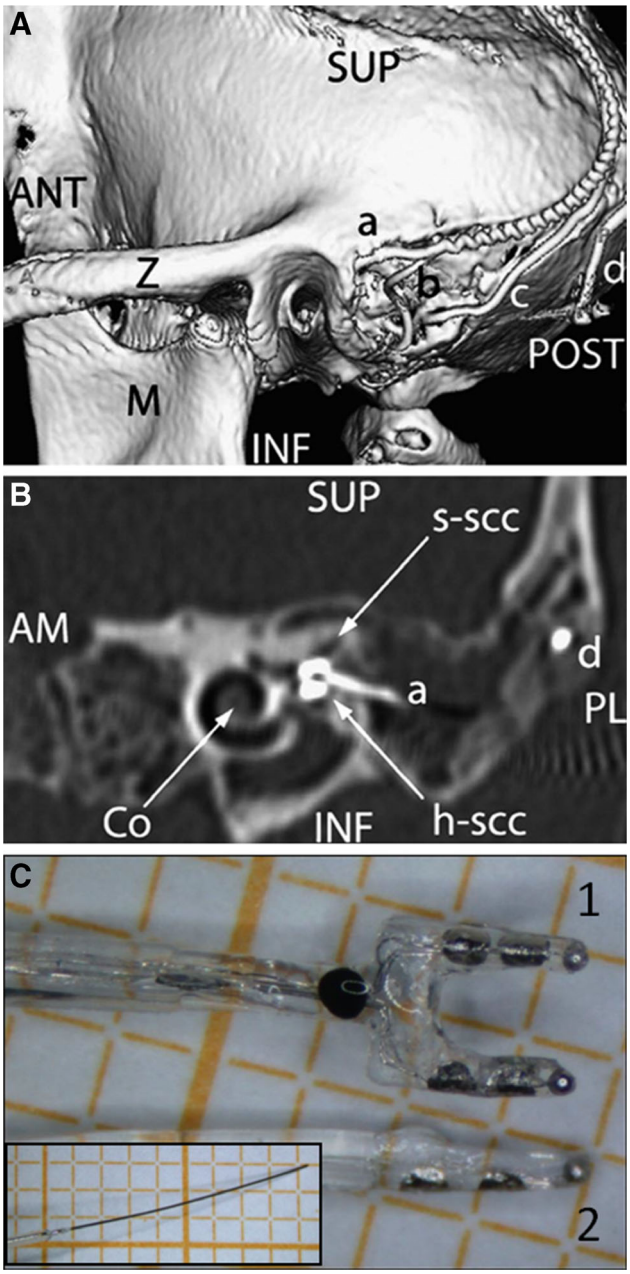

Fig. 7. Electrode array placement. **A** Posterolateral view of 3D CT surface reconstruction showing electrode array leads implanted in the left labyrinth of a rhesus monkey via the mastoid cavity. *a* lead to anterior and horizontal ampullae; *b* lead to posterior ampulla; *c* common crus reference electrode; *d* neck reference electrode; *M* mandibular ramus; *Z* zygomatic arch; *ANT, POST, SUP, INF* anterior, posterior, superior, inferior. **B** Oblique CT cut through the plane of the basal turn of the cochlea [*Co*], showing bifurcated electrode array [*a*] entering the ampullae of the superior [*s-scc*] and horizontal [*h-scc*] semicircular canals. Part of the neck reference electrode [*d*] is also visible, but the posterior SCC electrode array is not included in this section. *AM, PL* anteromedial, posterolateral. **C** Image of forked electrode arrays for h-scc and s-scc ampullas (*1*), posterior SCC (*2*), and common crus reference (*inset*) electrodes. **A** and **B** reproduced with permission from Dai et al. 2011b.

REFERENCES

ABERCROMBIE M (1946) Estimation of nuclear population from microtome sections. Anat Rec 94:239–247

BAIRD RA, TORRES MA, SCHUFF NR (1993) Hair cell regeneration in the bullfrog vestibular otolith organs following aminoglycoside toxicity. Hear Res 65:164–174

BRANDT T (1996) Bilateral vestibulopathy revisited. Eur J Med Res 1:361–368

CAREY J (2004) Intratympanic gentamicin for the treatment of Meniere's disease and other forms of peripheral vertigo. Otolaryngol Clin North Am 37:1075–1090

CAREY J, DELLA SANTINA C (2010) Principles of applied vestibular physiology. In: Flint P (ed) Cummings otolaryngology: head and neck surgery. Elsevier, Amsterdam

CAREY JP, FUCHS AF, RUBEL EW (1996) Hair cell regeneration and recovery of the vestibuloocular reflex in the avian vestibular system. J Neurophysiol 76:3301–3312

CHIA SH, GAMST AC, ANDERSON JP, HARRIS JP (2004) Intratympanic gentamicin therapy for Meniere's disease: a meta-analysis. Otol Neurotol 25:544–552

CHIANG B, FRIDMAN GY, DAI C, RAHMAN MA, DELLA SANTINA CC (2011) Design and performance of a multichannel vestibular prosthesis that restores semicircular canal sensation in rhesus monkey. IEEE Trans Neural Syst Rehabil Eng 19:588–598

CROWE SJ, GUILD SR, POLVOGT LM (1934) Observations on the pathology of high-tone deafness. Bull Johns Hopkins Hosp 54:315

DAI C, FRIDMAN GY, DAVIDOVICS NS, CHIANG B, AHN JH, DELLA SANTINA CC (2011A) Restoration of 3D vestibular sensation in rhesus monkeys using a multichannel vestibular prosthesis. Hear Res 281:74–83

DAI C, FRIDMAN GY, DELLA SANTINA CC (2011B) Effects of vestibular prosthesis electrode implantation and stimulation on hearing in rhesus monkeys. Hear Res 277:204–210

DAI C, FRIDMAN GY, CHIANG B, RAHMAN MA, AHN J, DAVIDOVICS NS, DELLA SANTINA CC (2013) Directional plasticity rapidly improves 3D vestibulo-ocular reflex alignment in monkeys using a multichannel vestibular prosthesis. J Assoc Res Otolaryngol. 2013;14(6):863–877

DAVIDOVICS NS, FRIDMAN GY, CHIANG B, DELLA SANTINA CC (2011) Effects of biphasic current pulse frequency, amplitude, duration, and interphase gap on eye movement responses to prosthetic electrical stimulation of the vestibular nerve. Neural Syst Rehabil Eng IEEE Trans on 19:84–94

DAVIDOVICS N, RAHMAN M, DAI C, AHN J, FRIDMAN G, DELLA SANTINA C (2013) Multichannel vestibular prosthesis employing modulation of pulse rate and current with alignment precompensation elicits improved VOR performance in monkeys. J Assoc Res Otolaryngol 14:233–248

DELLA SANTINA C, MIGLIACCIO A, PATEL A (2005) Electrical stimulation to restore vestibular function development of a 3-d vestibular prosthesis. Conf Proc IEEE Eng Med Biol Soc 7:7380–7385

DELLA SANTINA CC, MIGLIACCIO AA, PATEL AH (2007A) A multichannel semicircular canal neural prosthesis using electrical stimulation to restore 3D vestibular sensation. IEEE Trans Biomed Eng 54:1016–1030

DELLA SANTINA CC, MIGLIACCIO AA, PATEL AH (2007B) A multichannel semicircular canal neural prosthesis using electrical stimulation to restore 3-d vestibular sensation. IEEE Trans Biomed Eng 54:1016–1030

DESAI SS, ZEH C, LYSAKOWSKI A (2005A) Comparative morphology of rodent vestibular periphery. I. Saccular and utricular maculae. J Neurophysiol 93:251–266

DESAI SS, ALI H, LYSAKOWSKI A (2005B) Comparative morphology of rodent vestibular periphery. II. Cristae ampullares. J Neurophysiol 93:267–280

FERNANDEZ C, LYSAKOWSKI A, GOLDBERG JM (1995) Hair-cell counts and afferent innervation patterns in the cristae ampullares of the squirrel monkey with a comparison to the chinchilla. J Neurophysiol 73:1253–1269

FRIDMAN GY, DAVIDOVICS NS, DAI C, MIGLIACCIO AA, DELLA SANTINA CC (2010) Vestibulo-ocular reflex responses to a multichannel vestibular prosthesis incorporating a 3D coordinate transformation for correction of misalignment. J Assoc Res Otolaryngol 11:367–381

GACEK RR, GACEK MR (2002) Results of singular neurectomy in the posterior ampullary recess. ORL J Otorhinolaryngol Relat Spec 64:397–402

GOLUB JS, TONG L, NGYUEN TB, HUME CR, PALMITER RD, RUBEL EW, STONE JS (2012) Hair cell replacement in adult mouse utricles after targeted ablation of hair cells with diphtheria toxin. J Neurosci 32:15093–15105

GOLUB JS, LING L, NIE K, NOWACK A, SHEPHERD SJ, BIERER SM, JAMEYSON E, KANEKO CR, PHILLIPS JO, RUBINSTEIN JT (2014) Prosthetic implantation of the human vestibular system. Otol Neurotol 35:136–147

GONG W, MERFELD DM (2000) Prototype neural semicircular canal prosthesis using patterned electrical stimulation. Ann Biomed Eng 28:572–581

GONG W, MERFELD DM (2002) System design and performance of a unilateral horizontal semicircular canal prosthesis. IEEE Trans Biomed Eng 49:175–181

GOPEN Q, LOPEZ I, ISHIYAMA G, BALOH RW, ISHIYAMA A (2003) Unbiased stereologic type I and type II hair cell counts in human utricular macula. Laryngoscope 113:1132–1138

GUYOT J-P, SIGRIST A, PELIZZONE M, KOS MI (2011) Adaptation to steady-state electrical stimulation of the vestibular system in humans. Ann Otol Rhinol Laryngol 120:143–149

HIRVONEN TP, MINOR LB, HULLAR TE, CAREY JP (2005) Effects of intratympanic gentamicin on vestibular afferents and hair cells in the chinchilla. J Neurophysiol 93:643–655

IGARASHI M, MCLEOD ME, GRAYBIEL A (1965) Clinical pathological correlations in squirrel monkeys after suppression of semicircular canal function by streptomycin sulfate. Acta Otolaryngol. 1966;Suppl 214:1–28

ISHIYAMA G, LOPEZ I, BALOH RW, ISHIYAMA A (2007) Histopathology of the vestibular end organs after intratympanic gentamicin failure for Meniere's disease. Acta Otolaryngol 127:34–40

KIM HJ, LEE JO, KOO JW, KIM JS, BAN J (2013) Gentamicin-induced bilateral vestibulopathy in rabbits: vestibular dysfunction and histopathology. Laryngoscope 123:E51–58

KOS MI, FEIGL G, ANDERHUBER F, WALL C, FASEL JH, GUYOT JP (2006) Transcanal approach to the singular nerve. Otol Neurotol 27:542–546

LEWIS RF, HABURCAKOVA C, GONG W, MAKARY C, MERFELD DM (2010) Vestibuloocular reflex adaptation investigated with chronic motion-modulated electrical stimulation of semicircular canal afferents. J Neurophysiol 103:1066–1079

LINDEMAN HH (1969) Regional differences in sensitivity of the vestibular sensory epithelia to ototoxic antibiotics. Acta Otolaryngol 67:177–189

LOPEZ I, HONRUBIA V, LEE SC, SCHOEMAN G, BEYKIRCH K (1997) Quantification of the process of hair cell loss and recovery in the chinchilla crista ampullaris after gentamicin treatment. Int J Dev Neurosci 15:447–461

LOPEZ I, ISHIYAMA G, TANG Y, TOKITA J, BALOH RW, ISHIYAMA A (2005) Regional estimates of hair cells and supporting cells in the human crista ampullaris. J Neurosci Res 82:421–431

LYFORD-PIKE S, VOGELHEIM C, CHU E, DELLA SANTINA CC, CAREY JP (2007) Gentamicin is primarily localized in vestibular type I hair cells after intratympanic administration. J Assoc Res Otolaryngol 8:497–508

Lysakowski A, Goldberg JM (2008) Ultrastructural analysis of the cristae ampullares in the squirrel monkey (Saimiri sciureus). J Comp Neurol 511:47–64

Merchant SN (1999) A method for quantitative assessment of vestibular otopathology. Laryngoscope 109:1560–1569

Merchant SN, Velazquez-Villasenor L, Tsuji K, Glynn RJ, Wall C 3rd, Rauch SD (2000) Temporal bone studies of the human peripheral vestibular system. Normative vestibular hair cell data. Ann Otol Rhinol Laryngol Suppl 181:3–13

Minor LB (1998) Gentamicin-induced bilateral vestibular hypofunction. JAMA 279:541–544

Mitchell DE, Dai C, Rahman MA, Ahn JH, Della Santina CC, Cullen KE (2013) Head movements evoked in alert rhesus monkey by vestibular prosthesis stimulation: implications for postural and gaze stabilization. PLoS One 8:e78767

Nadol JJ (1981) Histopathology of human aminoglycoside ototoxicity. In: Lerner S, Matz G, Hawkins JJ (eds) Aminoglycoside ototoxicity. Little, Brown, Boston, pp 409–435

Nadol JB Jr, Eddington DK (2006) Histopathology of the inner ear relevant to cochlear implantation. Adv Otorhinolaryngol 64:31–49

Nadol JB Jr, Eddington DK, Burgess BJ (2008) Foreign body or hypersensitivity granuloma of the inner ear after cochlear implantation: one possible cause of a soft failure? Otol Neurotol 29:1076–1084

Nguyen KD, Minor LB, Della Santina CC, Carey JP (2009) Vestibular function and vertigo control after intratympanic gentamicin for Ménière's disease. Audiol Neurotol 14:361–372

O'Leary SJ, Monksfield P, Kel G, Connolly T, Souter MA, Chang A, Marovic P, O'Leary JS, Richardson R, Eastwood H (2013) Relations between cochlear histopathology and hearing loss in experimental cochlear implantation. Hear Res 298:27–35

Perez Fornos A, Guinand N, van de Berg R, Stokroos R, Micera S, Kingma H, Pelizzone M, Guyot JP (2014) Artificial balance: restoration of the vestibulo-ocular reflex in humans with a prototype vestibular neuroprosthesis. Front Neurol 5:66

Rauch SD, Velazquez-Villasenor L, Dimitri PS, Merchant SN (2001) Decreasing hair cell counts in aging humans. Ann N Y Acad Sci 942:220–227

Richter E (1980) Quantitative study of human Scarpa's ganglion and vestibular sensory epithelia. Acta Otolaryngol 90:199–208

Rubinstein JT (2014) Human longitudinal studies of electrical stimulation of the vestibular periphery. In 13th International Conference on Cochlear Implants and Other Implantable Auditory Technologies, Munich

Rubinstein JT, Bierer S, Kaneko C, Ling L, Nie K, Oxford T, Newlands S, Santos F, Risi F, Abbas PJ et al (2012) Implantation of the semicircular canals with preservation of hearing and rotational sensitivity: a vestibular neurostimulator suitable for clinical research. Otol Neurotol 33:789–796

Schuknecht H (1993) Pathology of the ear. Lea & Febiger, Philadelphia

Sera K, Harada Y, Tagashira N, Suzuki M, Hirakawa K, Ohya T (1987) Morphological changes in the vestibular epithelia and ganglion induced by ototoxic drug. Scanning Microsc 1:1191–1197

Severinsen SA, Sorensen MS, Kirkegaard M, Nyengaard JR (2010) Stereological estimation of total cell numbers in the young human utricular macula. Acta Otolaryngol 130:773–779

Shepherd RK, Webb RL, Clark GM, Pyman BC, Hirshorn MS, Murray MT, Houghton ME (1984) Implanted material tolerance studies for a multiple-channel cochlear prosthesis. Acta Otolaryngol Suppl 411:71–81

Sterio DC (1984) The unbiased estimation of number and sizes of arbitrary particles using the disector. J Microsc 134:127–136

Stokroos R, van de Berg R, Perez-Fornos A, Guinand N, Kingma H, Guyot J (2014) Vestibular implant surgery: progression and pitfalls. In 13th International Conference on Cochlear Implants and Other Implantable Auditory Technologies, Munich

Sun DQ, Ward BK, Semenov YR, Carey JP, Della Santina CC (2014) Bilateral vestibular deficiency: quality of life and economic implications. JAMA Otolaryngol Head Neck Surg 140(6):527–534

Tien HC, Linthicum FH Jr (2002) Histopathologic changes in the vestibule after cochlear implantation. Otolaryngol Head Neck Surg 127:260–264

Tsuji K, Velazquez-Villasenor L, Rauch SD, Glynn RJ, Wall C 3rd, Merchant SN (2000) Temporal bone studies of the human peripheral vestibular system. Aminoglycoside ototoxicity. Ann Otol Rhinol Laryngol 109:20–25

Uchino Y, Isu N, Ichikawa T, Satoh S, Watanabe S (1988) Properties and localization of the anterior semicircular canal-activated vestibulocollic neurons in the cat. Exp Brain Res 71:345–352

van de Berg R, Guinand N, Guyot JP, Kingma H, Stokroos RJ (2012) The modified ampullar approach for vestibular implant surgery: feasibility and its first application in a human with a long-term vestibular loss. Front Neurol 3:18

Wall C 3rd, Merfeld DM, Rauch SD, Black FO (2002) Vestibular prostheses: the engineering and biomedical issues. J Vestib Res 12:95–113

Wall C 3rd, Kos MI, Guyot JP (2007) Eye movements in response to electric stimulation of the human posterior ampullary nerve. Ann Otol Rhinol Laryngol 116:369–374

Wersall J, Hawkins JE Jr (1962) The vestibular sensory epithelia in the cat labyrinth and their reactions in chronic streptomycin intoxication. Acta Otolaryngol 54:1–23

Wilson VJ, Yamagata Y, Yates BJ, Schor RH, Nonaka S (1990) Response of vestibular neurons to head rotations in vertical planes. III. Response of vestibulocollic neurons to vestibular and neck stimulation. J Neurophysiol 64:1695–1703